scientific reports

Check for updates

OPEN

Single-cell RNA sequencing reveals potential therapeutic targets in the tumor microenvironment of lung squamous cell carcinoma

Junda Fan[1,7], Yu Chen[2,7], Yue Gong[3], Hongmei Sun[4], Rui Hou[3], Xiaoya Dou[3], Yanping Zhang[5] & Cheng Huo[6]✉

Lung squamous cell carcinoma (LUSC), accounting for 30% of lung cancer cases, lacks adequate research due to limited understanding of its molecular abnormalities. Our study analyzed public LUSC datasets to explore the tumor microenvironment (TME) composition using scRNA-seq from two cohorts. Applying non-negative matrix factorization, we identified unique malignant cell phenotypes, or meta-programs (MPs), based on gene expression patterns. Survival analysis revealed the clinical relevance of these MPs. Findings illuminated a TME landscape enriched with immune cells—CD8 + T, exhausted T, CD4 + T, and naive T cells—and suggested roles for myeloid cells, like cDC1 and pDCs, in LUSC progression. Different MPs highlighted the heterogeneity of malignant cells and their clinical implications. Targeting MP-specific genes may enable personalized therapy, especially for early-stage LUSC. This study offers insights into immune cell function in tumor dynamics, identifies MPs, and paves the way for novel LUSC strategies, enhancing early intervention, personalized treatment, and prognosis, ultimately improving patient outcomes.

Keywords Single-cell RNA sequencing, Lung cancer, Tumor microenvironment, Non-negative matrix factorization, Bioinformatics

Lung squamous cell carcinoma (LUSC) constitutes approximately 30% of all lung cancer cases and is a leading cause of cancer-related mortality worldwide[1]. Despite its prevalence, LUSC has received comparatively less attention in research and clinical practice when compared to lung adenocarcinoma and other major cancer types[2–6]. The clinical staging of LUSC is primarily determined by factors such as tumor size, lymph node involvement, and the presence of metastasis[2]. These staging criteria play a crucial role in guiding treatment strategies and predicting patient prognosis[7]. However, it is important to note that even within the same stage, patients with LUSC often exhibit substantial variations in clinical outcomes. This observation underscores the limitations of the current staging methods employed in LUSC management.

To address these limitations and improve patient care, by incorporating additional factors that influence disease progression and patient outcomes, such as molecular markers or genetic alterations, we can potentially enhance the accuracy of prognostic predictions and tailor treatment strategies accordingly[8]. This approach allows us to capture the complexity of the tumor microenvironment (TME), which comprises diverse immune cells, fibroblasts, endothelial cells, and other components [9,10]. In particular, the composition and functional states of immune cells within the TME have been demonstrated to exert a profound influence on prognosis and the efficacy of immunotherapy in the context of lung cancer [11,12]. However, existing staging methods for LUSC lack the necessary resolution to comprehensively characterize the TME specific to LUSC.

Single-cell RNA sequencing (scRNA-seq) has emerged as a powerful technique for investigating gene expression patterns at a high resolution within tumor samples [13,14]. This technology enables the profiling of thousands to millions of individual cells, providing valuable insights into the composition, activation states, and interactions of cells within the TME[15]. By leveraging scRNA-seq data, novel cellular and genetic signatures

[1]Department of Oncology, 242 Hospital Affiliated to Shenyang Medical College, Shenyang 110034, China. [2]Jiamusi Central Hospital, Jiamusi 154000, China. [3]Geneis Beijing Co., Ltd, Beijing 100102, China. [4]Department of Medical Oncology, The Cancer Hospital of Jia Mu Si, Jiamusi 154000, China. [5]School of Mathematics and Physics Science and Engineering, Hebei University of Engineering, Handan 056038, China. [6]Departmen of Pathology, Sinopharm Tongmei General Hospital, Datong 037003, China. [7]Junda Fan and Yu Chen contributed equally to this work. ✉email: huocheng_tmzy@163.com

that can enhance the staging, treatment selection, and prognostic prediction of patients with LUSC, going beyond the limitations of histopathological features alone[16]. Numerous studies have utilized scRNA-seq to establish correlations between immune cell fractions, gene expression profiles, and prognosis or response to immunotherapy in various cancer types [17–19]. For example, Salcher performed an integrative analysis on 1,283,972 single cells from 556 samples and 318 Non-small cell lung cancer (NSCLC) patients across 29 datasets[20]. By focusing on tissue-resident neutrophils (TRNs), they identified cell populations that develop novel functional properties in tissue TME. Finally, they uncovered a TRN-derived signature, playing significant roles in the failure of anti-programmed cell death ligand 1 (PD-L1) treatment. These investigations have shed light on the complex interplay between the immune system and tumor cells, offering potential avenues for improving patient outcomes. However, a comprehensive characterization of TME in LUSC is more or less ignored.

In this study, we aim to comprehensively characterize the TME in LUSC using scRNA-seq technology. Through an in-depth investigation into the cellular composition of the TME, we aim to elucidate the intricate interplay between TME and the immune and stromal cells. Moreover, by identifying distinct malignant cell phenotypes, we intend to shed light on the potential clinical implications of these findings and pave the way for the development of targeted therapies specifically tailored for LUSC patients, with a particular focus on those in the early stages of the disease. Additionally, the biomarkers identified in this study hold promise for their potential utilization in predicting patient prognosis, thus further enhancing the clinical significance of our research.

Results

Identification of the microenvironment in the LUSC tumors based on single-cell sequencing data analysis

We downloaded lung cancer datasets from GSE148071 and WCH, screened out 72 LUSC samples (22 from GSE148071 and 50 from WCH) and merged them together (Fig. 1a). A total of 179,506 cells were obtained from 72 samples for downstream analysis. The median number of expressed genes in each cell for GSE148071 and WCH were 1450 and 362 respectively (Table S1). The top 2,000 highly variable genes were identified and used for principal component analysis (PCA) and uniform manifold approximation and projection (UMAP) analysis (Fig. 1a). Top 20 principal components were correct by Harmony[21] and the neighborhood graph was constructed by BBKNN[22]. By performing the Leiden algorithm[23] on the neighborhood graph, 19 high-confidence cell clusters were identified with a resolution of 0.8. These clusters were broadly classified into seven major cell types using specific markers from the original literature, including epithelial cells (EPCAM and KRT18), T cells (CD2, CD3D, CD3E and CD3G), B cells (CD79A and CD79B), myeloid cells (LYZ), endothelial cells (CLDN5, PECAM1 and VWF), mast cells (TPSAB1, TPSB2 and GATA2), and fibroblasts (DCN, COL1A1 and COL1A2) (Fig. 1b).

In order to distinguish malignant cells from non-malignant cells confidently, we assessed large-scale chromosomal copy-number variations (CNVs) in each individual cell. Our hypothesis was that cells exhibiting a high degree of CNVs were likely to be indicative of malignancy. To infer the CNV content of individual cells from scRNA-seq data, we utilized a sliding window approach implemented by the infercnvpy package[24]. Compared to normal reference cells, such as T cells, B cells, myeloid cells and mast cells, a subset of epithelial cells showed a significantly higher CNV burden. By clustering the 179,506 cells based on their CNV profiles, we were able to identify 9,611 malignant cells from the non-malignant epithelial cells (Fig. 1c&d).

Analysis of cellular architectures across tumor stages

To explore the propensity of specific cell types during cancer progression, we compared the ratios of cell types present in tumor samples across different tumor stages (Fig. 2a and b). Our results demonstrated a significantly higher proportion of malignant cells in tumors from the advanced tumor stages, suggesting a high degree of tumor deterioration in patients with later-stage cancer. Mast cells play a crucial role in the tumor microenvironment[25]. Their functions include modulating immune responses, promoting angiogenesis, and influencing tumor progression. The observed decrease in mast cell numbers from Stage II to advanced stages warrants further exploration. Potential reasons could involve changes in the tumor microenvironment[26], immune suppression[27], or altered signaling pathways[28]. Similarly, the prominence of fibroblasts at Stage IV is intriguing. These cells are key players in the tumor stroma, affecting extracellular matrix remodeling[29], immune cell recruitment[30], and tumor growth[31]. Discussing their role and potential implications in advanced LUSC stages is essential. Additionally, the proportion of T cells has a clear decreasing trend correlated with the development of cancer, indicating that impaired anti-tumor immune surveillance may facilitate cancer advancement. For epithelial cells, the proportion is lower in the adjacent tissues but higher in the samples from intermediate and late tumor stages. Additionally, these results were verified by Propeller method (Table S2). Taken together, these findings suggest that certain cell types play critical roles in driving cancer development at different stages, further subdivision and detailed analysis of cellular subpopulations is warranted to better understand how distinct cell types influence cancer progression as tumors evolve over time.

Immunosuppressive adaptations in the late-atage LUSC TME collectively dampen the anti-tumor immune response

We first characterized the subpopulations in tumor-infiltrating T cells across LUSC stages. By re-clustering T cells, we identified seven T cell subsets, including CD4 + T cells (S100A9, SLPI), regulator T cells (FOXP3, IL2RA and TNFRSF4), exhausted T cells (LAG3, ZNF683 and CXCL13), CD8 + T cells (GZMK and CCL4L2), NK cells (KLRD1, GNLY and KLRB1), naïve T cells (GPX2, PERP, KRT17), and helper T cells (IL7R, CD6) (Fig. 3a and S1a).

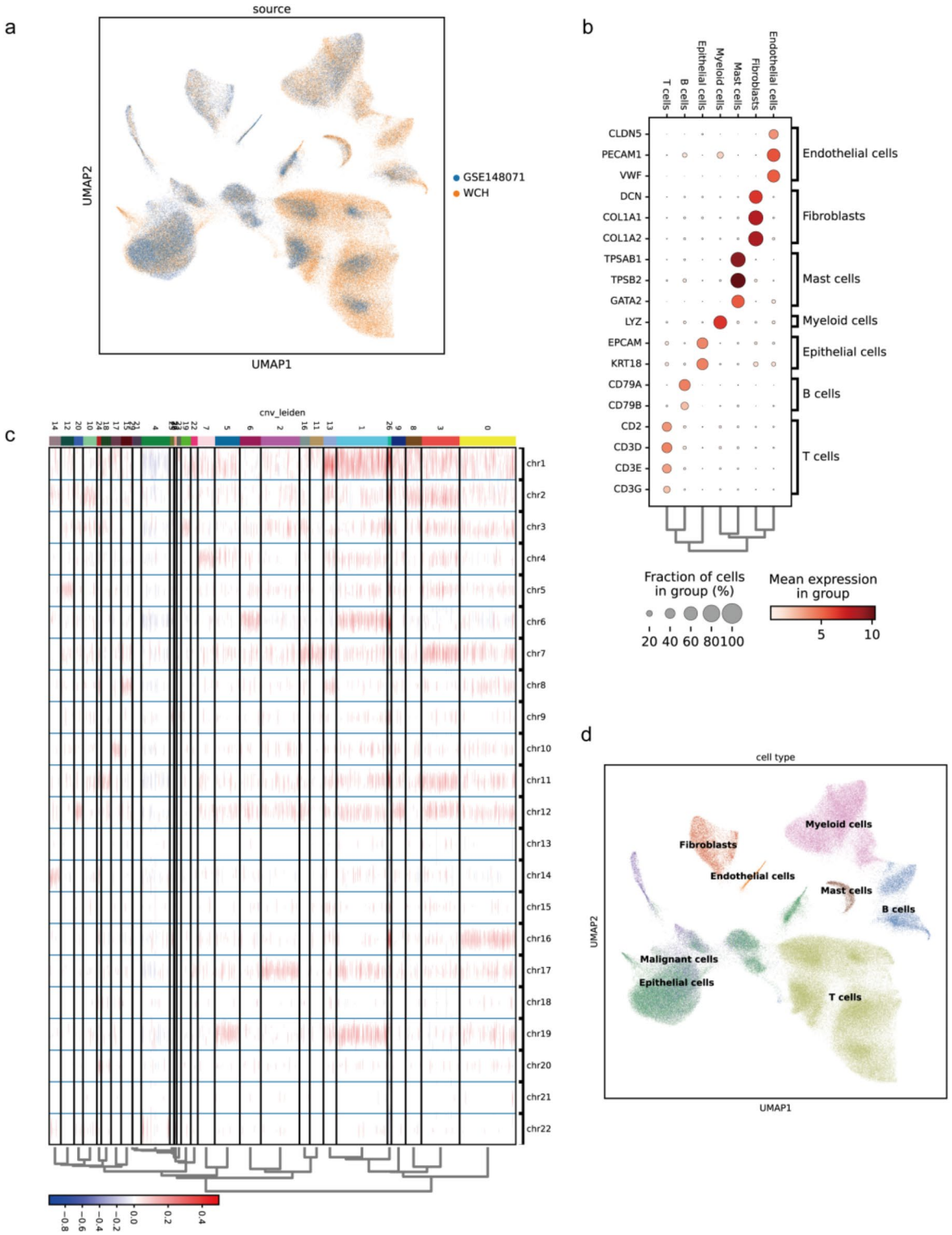

Fig. 1. Identification of cellular composition in the tumor microenvironment (TME) of lung squamous cell carcinoma (LUSE) from two independent cohorts. (**a**) Projection of all cells from the two cohorts into a UMAP (Uniform Manifold Approximation and Projection) space, with cells colored by their sources. (**b**) Unsupervised clustering reveals major cell types in the merged dataset, with cells in the UMAP plot colored according to their respective cell types. (**c**) Heatmap visualization of inferred copy number variation (CNV) profiles for each cell, based on transcriptomic data. The colorbar at the top of the heatmap represents the clustering result of cells based on their CNV profiles. (**d**) Dotplot displaying marker genes identified in the major cell types within the merged dataset. The size of each dot indicates the expression prevalence of the corresponding gene, while the dot color represents the average expression of the gene across the entire population of the corresponding cell type.

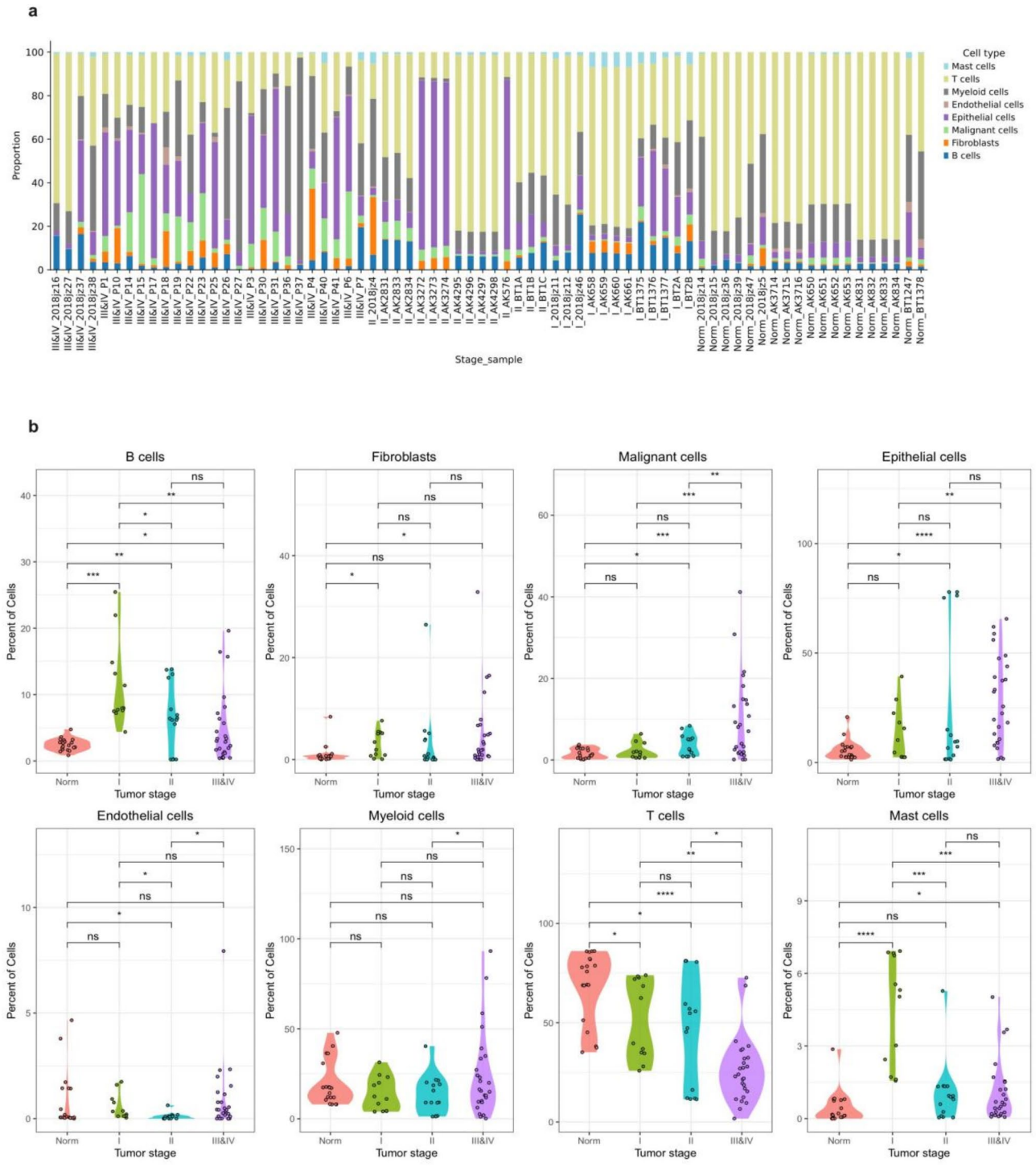

Fig. 2. Analysis of Cellular Proportions in the LUSC TME. (**a**) Stacked barplot illustrating the major cell types present in all tumor samples included in this study. The samples are ordered by disease stage, and the color represents the corresponding cell type. The height of each color within a sample indicates the proportion of that specific cell type. (**b**) Violin plots depicting the proportions of the given cell type in samples from different tumor stages. A t-test was performed to assess the statistical significance of differences in cell type proportions between the two tumor stages.

While previous studies linked increased cytotoxic T cell infiltration to improved outcomes[32], we observed decreasing CD8 + and exhausted T cell fractions concurrently with disease progression (Fig. 3b and S1b). As CD8 + and exhausted T cells mediate the direct killing of malignant cells, their decline late in tumorigenesis permits the escape of malignant cells from immune-mediated control[33]. Intriguingly, the fraction of regulatory T cell remained stable even as other subpopulations changed. This stability likely stems from tumor-secreted factors

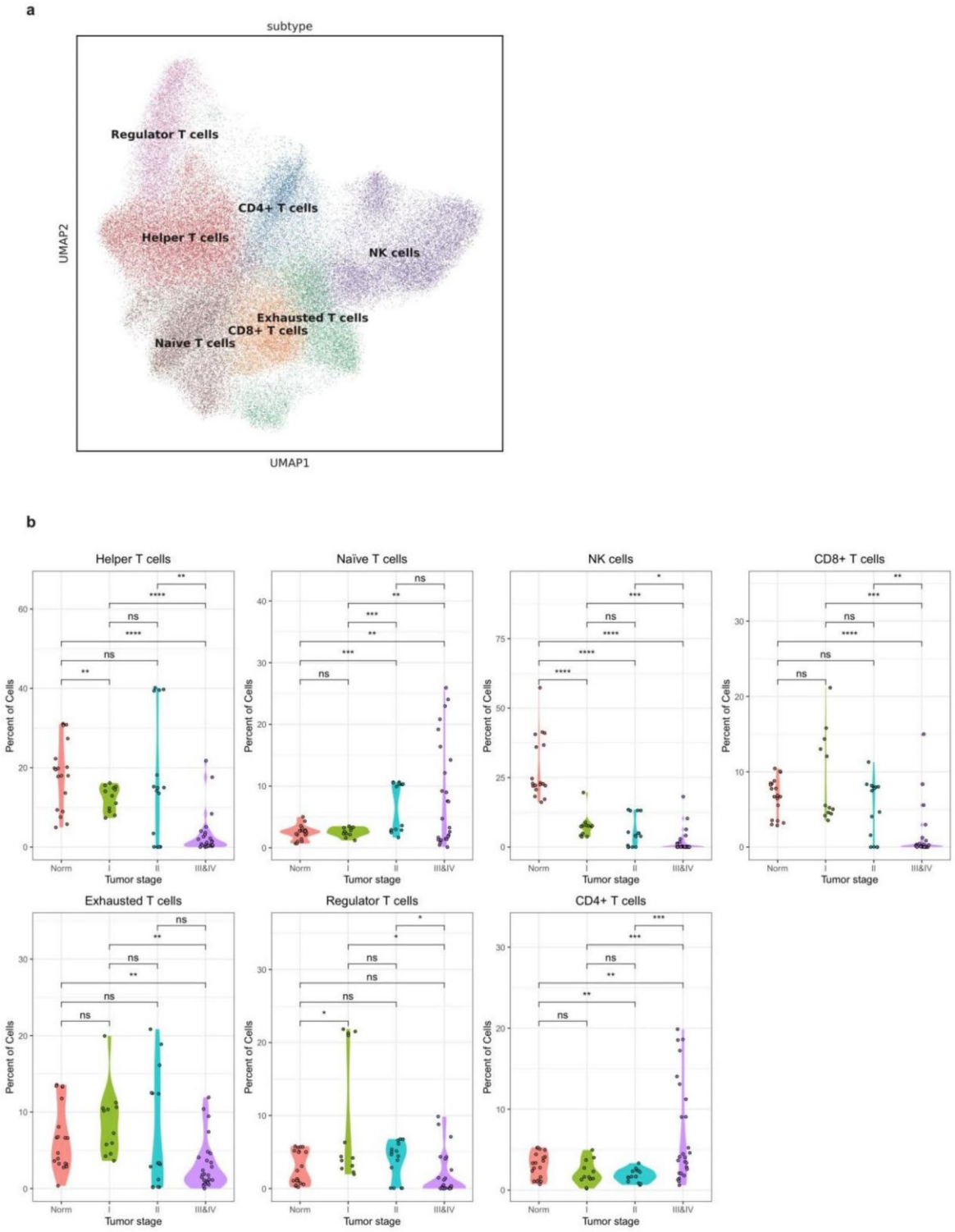

Fig. 3. The exploration of T cells within the TME of LUSC. (**a**) UMAP plot illustrating the identification of 7 distinct T cell subpopulations using the Leiden algorithm in this investigation. (**b**) Violin plots presenting the relative proportions of the specific T cell subpopulation in samples from various tumor stages. Statistical significance of differences in cell type proportions between the two tumor stages was evaluated using a t-test.

that actively maintain regulatory T cell immunosuppressive influence within the TME of LUSC. By dampening anti-tumor immune responses, regulatory T cells may compensate for decreasing CD8 + and exhausted T cell activity in advanced stages [3,34,35].

In further contrast, CD4 + T cell and naive T cell proportions increased as cancer developed (Fig. 3b and S1b). As CD4 + T cells can enhance regulatory effects and dampen cytotoxic functions, the elevated level of CD4 + T cell may facilitate immune evasion [36,37]. Naive T cell accumulation may reflect impaired priming of effective anti-tumor responses. The results of the Propeller method also confirmed that the proportions of CD4 + T cells and naive T cells increased in advanced tumors (Table S3).

Identification of myeloid cell subpopulations in late-stage lung squamous cell carcinoma

In LUSC, the role of myeloid cells in tumor progression and immune evasion is poorly understood. To address this gap in knowledge, we reclustered meyloid cells and identified six subpopulations, including conventional type 1 dendritic cells (cDC1) (C1orf54, WDFY4 and CLEC9A), conventional type 2 dendritic cells (cDC2) (FCER1A, CD1C), plasmacytoid dendritic cells (pDC) (IL3RA, LILRA4 and JCHAIN), myeloid dendritic cells (mDC) (LAMP3), monocytes (FCN1, CD300E and VCAN) and macrophages (APOE, APOC1 and CCL18), distinguished by the expression of their marker genes (Fig. 4a and S2a).

By comparing the myeloid cell composition across patients, we observed that samples of late tumor stages (stage III and IV) tended to have a higher proportion of myeloid cells (Fig. 4b and S2b). However, the compositions of the 3 subpopulations (cDC2, mDC, and macrophage) in the samples with different tumor stages were not significantly different (Fig. 4b and S2b). This suggests that the relative proportions of these subpopulations may not be strongly associated with tumor stage in LUSC.

Interestingly, normal samples exhibit a significantly bigger fraction of cDC1 (p-value = 1.04×e-9 between different stages, one-way ANOVA test) than tumor samples (Fig. 4b and S2b), suggesting that cDC1 may play a anti-tumor role and may be suppressed in the initiation of the LUSC. Previous studies have shown that cDC1 cells are potent inducers of anti-tumor immunity and are critical for the activation of CD8 + T cells, which are important effectors of the anti-tumor response[38]. Therefore, our findings suggest that cDC1 cells may represent a promising therapeutic target for LUSC and warrant further investigation. According to the Propeller results, we observed a significant increase in the proportion of cDC1 in normal samples compared to tumor tissues (Table S4).

Meanwhile, we found that pDC was uniquely enriched in the Stage II of LUSC (Fig. 4b, S2b **and** Table S4), which could potentially serve as a biomarker for LUSC staging. It has been suggested that pDCs can promote tumor growth and metastasis by suppressing the anti-tumor immune response through the secretion of immunosuppressive cytokines and the induction of regulatory T cells[39]. However, the exact mechanisms underlying the enrichment of pDCs in Stage II of LUSC remain to be elucidated.

Furthermore, our analysis revealed that monocyte gradually expanded their population along the cancer progression (Fig. 4b, S2b **and Table S4**). Monocytes are known to differentiate into macrophages [40,41], which play a critical role in cancer progression by promoting tumor growth, angiogenesis, and metastasis[42]. In the context of LUSC, the gradual expansion of monocytes along cancer progression suggests the balance between macrophages may shift, which could promote tumor growth, angiogenesis, and metastasis, as well as immune evasion[43]. Indeed, previous studies have shown that tumor-associated macrophages are associated with poor prognosis in LUSC and other cancers [14,44].

Epithelial cells analysis in LUSC

LUSC arises from epithelial cells[45]. Previous studies have indicated that different subtypes of epithelial cells in the lung play diverse roles in tissue function[46]. However, the specific roles of these subpopulations in LUSC progression remain unclear. In this work, we observed that epithelial cell has a higher proportion in the samples of the middle and late tumor stages (Fig. 2a**&b**). By reclustering epithelial cells, we divided them into six subpopulations, including alveolar type I (AT1) cells (AGER, CLIC5 and RTKN2), alveolar type II (AT2) cells (SFTPA1, ABCA3, PGC and SFTPA2), basal cells (KRT5, KRT6A, KRT14 and KRT17), club cells (SCGB1A1, SCGB3A1 and PIGR), ciliated cells (FOXJ1, TPPP3, PIFO, C11orf88 and DTHD1), and deuterosomal cells (CDC20 and CCNO) (Fig. 5a and S3a).

Among the six subpopulations, deuterosomal cells and basal cells showed a significant increase in proportion in samples from moderate to advanced cancer (Fig. 5b and S3b). With the progression of tumors, an increase in the proportion of deuterosomal cells was also observed using the Propeller method (Table S5). This suggests that these subpopulations may be involved in LUSC tumor development and progression. Deuterosomal cells are a type of epithelial cell that have been shown to play a role in tissue repair and regeneration[47]. The significant increase in their proportion in LUSC samples suggests that they may also be involved in tumor progression. Meanwhile, previous studies have suggested that basal cells may have stem cell-like properties and be involved in lung cancer development[48]. Still, the specific mechanisms underlying the involvement of these subpopulations in LUSC development and progression is unclear.

Characterization of intratumor heterogeneity among malignant cells using scRNA data and NMF programs

Malignant cells are known to exhibit a high degree of intratumor heterogeneity, with different cells displaying varying phenotypes and functions depending on their genetic mutations and the microenvironment of the tumor[49]. In order to gain a better understanding of this intratumor heterogeneity, we utilized scRNA data to cluster malignant cells. To achieve this, we employed non-negative matrix factorization (NMF) to identify NMF programs among malignant cells for each tumor sample. Through this approach, we were able to identify 468 NMF programs, with each program being summarized by the top 50 genes based on their NMF coefficients.

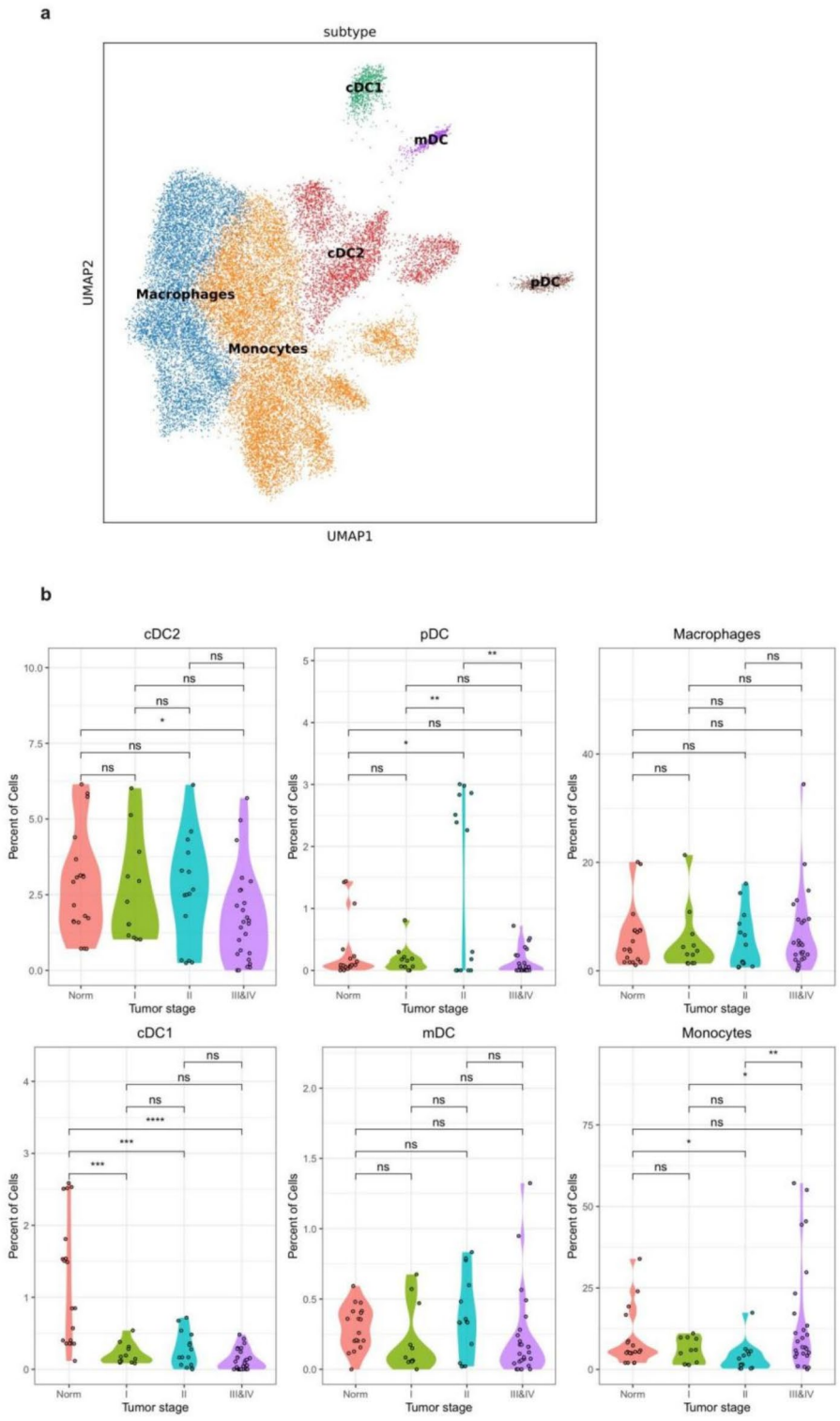

Fig. 4. The subpopulations of myeloid cells present in the TME of LUSC. (**a**) UMAP plot demonstrating the identification of all myeloid cell subpopulations using unsupervised clustering. (**b**) Violin plots displaying the relative proportions of the specific myeloid cell subpopulation in samples from different tumor stages. The statistical significance of differences in cell type proportions between the two tumor stages was assessed using a t-test.

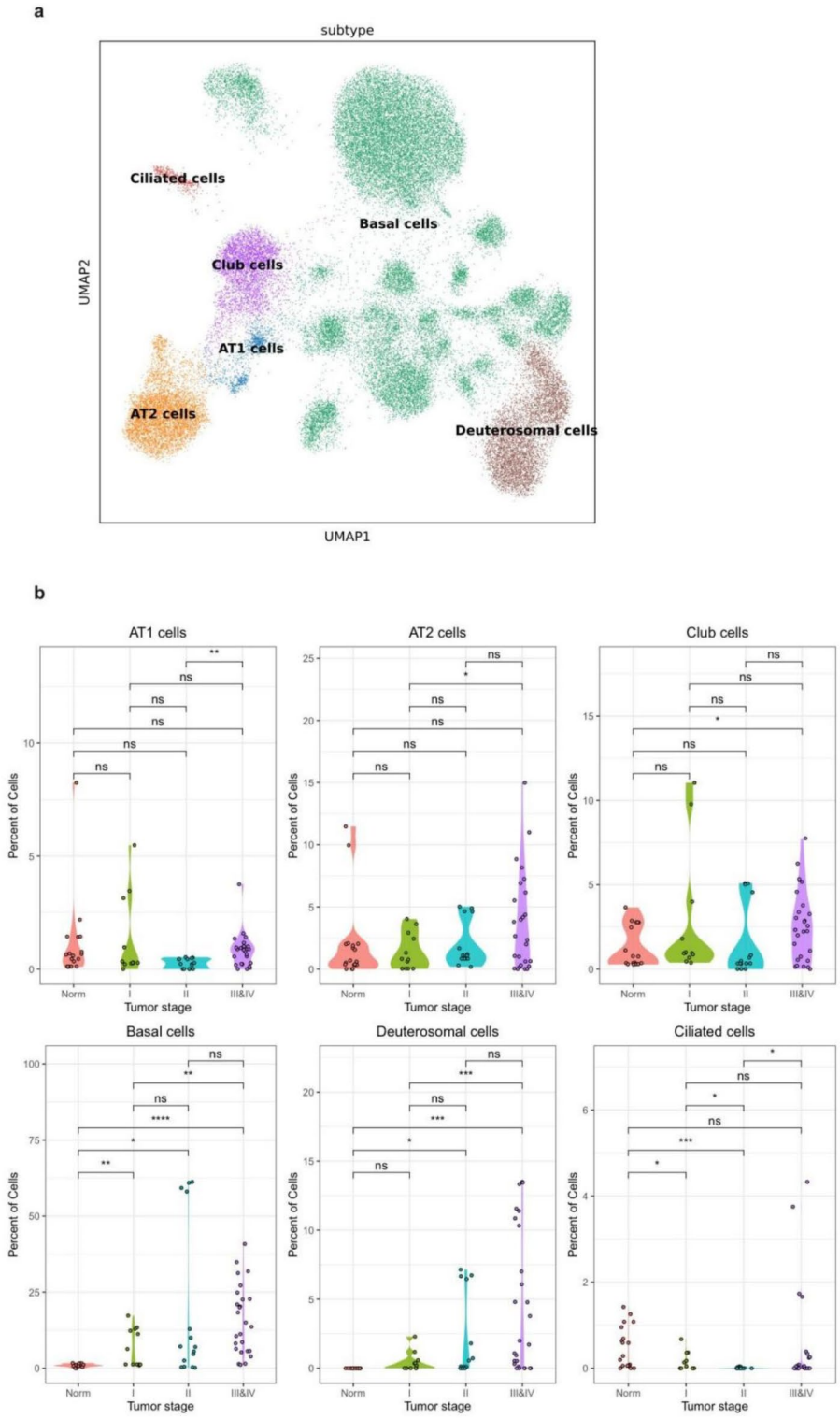

Fig. 5. Characterization of epithelial cell subpopulations in the tumor microenvironment (TME) of LUSC. (**a**) UMAP plot demonstrating the identification of 6 distinct epithelial cell subpopulations through the application of the Leiden algorithm in this study. (**b**) Violin plots displaying the relative proportions of specific epithelial cell subpopulations in samples from different tumor stages. Statistical analysis using a t-test was conducted to evaluate the significance of differences in cell type proportions between the two tumor stages.

Given the patient-specific nature of genetic mutations in malignant cells, we focused on identifying general NMF programs that could be found across multiple patients, with the aim of developing treatments that are effective for the majority of patients with LUSC.

We found that many NMF programs shared the top genes, indicating that they were derived from the same meta-programs (MPs). We clustered the NMF programs based on their fractions of shared top genes and defined clusters with more than 5 NMF programs as an MP. In total, we identified 4 MPs, each represented by the union of genes from the associated NMF programs (Fig. S4). We then annotated each MP based on the functional enrichments of representative genes (Fig. 6a-d). MP1 was found to be enriched in microtubule-based movement, suggesting that it may be involved in cellular processes related to cancer metastasis[50]. MP2 displayed up-regulation of ribosome-related genes, which may indicate an increase in ribosome biogenesis and a higher demand for protein synthesis to support the rapid growth and division of cancer cells[51]. MP3 was potentially involved in the formation of the cornified envelope, which could be a sign of cancer cells adapting to their environment and evading the immune system or other treatments[52]. MP4 displayed up-regulation of cell cycle-related activities, indicating that these cells were dividing and proliferating more rapidly than normal cells, a hallmark of cancer [53,54]. The identification of MPs enabled the characterization of intratumor heterogeneity among malignant cells in LUSC patients. The MPs represent distinct phenotypes of malignant cells within the tumor, and the genes that are representative of each MP can be targeted for the development of effective treatments for LUSC patients.

Clinical significance of MPs presented in LUSC

To further investigate the utility of the MPs identified in this study, we scored all bulk RNA-seq sample of LUSC from the TCGA-cohort using the representative genes of each MP (the union of top 50 genes in all associated NMF programs). For a bulk RNA-seq sample, we labeled it with the MP whose score was the highest in the sample. As a result, all tumor samples were labeled as either MP2 or MP4 (Fig. 7a). Survival analysis indicated no differences in survival among patients in the MP2 and MP4 groups (Fig. 7b). We further divided the samples by stages and drew Kaplan-Meier (KM) curves of two group samples for each cancer stage separately. As shown in Fig. 7c-f, only samples in Stage I displayed significantly different OS time, suggesting that genes in MP2&4 may be a useful prognostic gene program for early-stage LUSC. These findings highlight the potential clinical significance of the MPs identified in this study. Targeting the genes that are representative of each MP could lead to the development of effective treatments for LUSC patients, particularly those with early-stage disease.

Discussion

In this study, we utilized scRNA-seq technology to analyze the TME of LUSC tumors. By surveying public scRNA-seq data, we identified the cellular composition and observed trends in cell type proportions across different tumor stages, indicating the involvement of specific cell types in cancer development. We further analyzed subpopulations to understand their influence on cancer progression.

During our investigation, we observed a significant decrease in T cells with cancer progression. Meanwhile, Fig. 1a indicates a higher representation of T cells in the WCH dataset relative to the GSE148071 dataset. This discrepancy in cell type distribution could indeed impact the interpretation of our findings. To mitigate this concern, we conducted a comparison of late-stage samples from both datasets, as depicted in Fig. 2a, demonstrating that the cellular composition of these late-stage samples is strikingly similar, which bolsters our confidence in the assertion that the observed changes in T cell fractions are more closely associated with tumor stage than with any inherent biases in our sampling methodology. The decrease in cytotoxic CD8 + T cells and the increase in exhausted T cells with advancing tumor stage (as shown in Fig. 3b) suggest an impaired anti-tumor immune response, which may contribute to tumor progression and metastasis. This finding is consistent with previous studies that have highlighted the critical role of CD8 + T cells in controlling tumor growth[55] and the negative impact of T cell exhaustion on clinical outcomes[56]. Moreover, the stable proportion of regulatory T cells (Tregs) across different stages (Fig. 3b) indicates their potential role in maintaining an immunosuppressive TME, which could facilitate immune evasion by LUSC cells[57]. The clinical significance of targeting Tregs has been previously discussed in the context of various cancers[58], and our findings support the need for further investigation into their role in LUSC.

As shown in Fig. 4b, he myeloid compartment, comprising cells such as cDCs, pDCs, and macrophages, plays a dual role in cancer—promoting anti-tumor immunity and facilitating immunosuppression[59,60]. Our findings indicate a notable increase in myeloid cells with advancing tumor stage, which may reflect the tumor's ability to recruit these cells to create a more immunosuppressive environment[61]. The decrease of cDC1 cells in tumors, which are known for their potent antigen-presenting capabilities and for activating cytotoxic T cells, suggests a dampening of the adaptive immune response in LUSC[62]. This finding is consistent with other studies that have shown a reduction in cDC1 infiltration in various solid tumors, correlating with poor prognosis[63]. On the other hand, the enrichment of pDCs in stage II of LUSC (as shown in Fig. 4b) is intriguing and may indicate a stage-specific immune response. pDCs have been shown to produce large amounts of type I interferons, which can have both anti-tumor and pro-tumor effects, depending on the context[64,65]. The increased presence of pDCs at this stage could potentially be exploited as a biomarker for early detection or as a target for immunotherapeutic intervention. Monocytes, as a component of the innate immune system, are known to infiltrate tumors and differentiate into macrophages or dendritic cells, depending on the local microenvironment[41]. The gradual increase in monocytes during LUSC progression suggests a potential role in the tumor's immune evasion and angiogenesis. This increase may reflect the tumor's ability to recruit monocytes to promote a more immunosuppressive environment, which could facilitate tumor growth and metastasis[66].

Furthermore, the increase in specific epithelial cell subpopulations (Fig. 5b), such as basal and deuterosomal cells, with advancing cancer stage is intriguing and warrants further investigation, Basal cells, with their

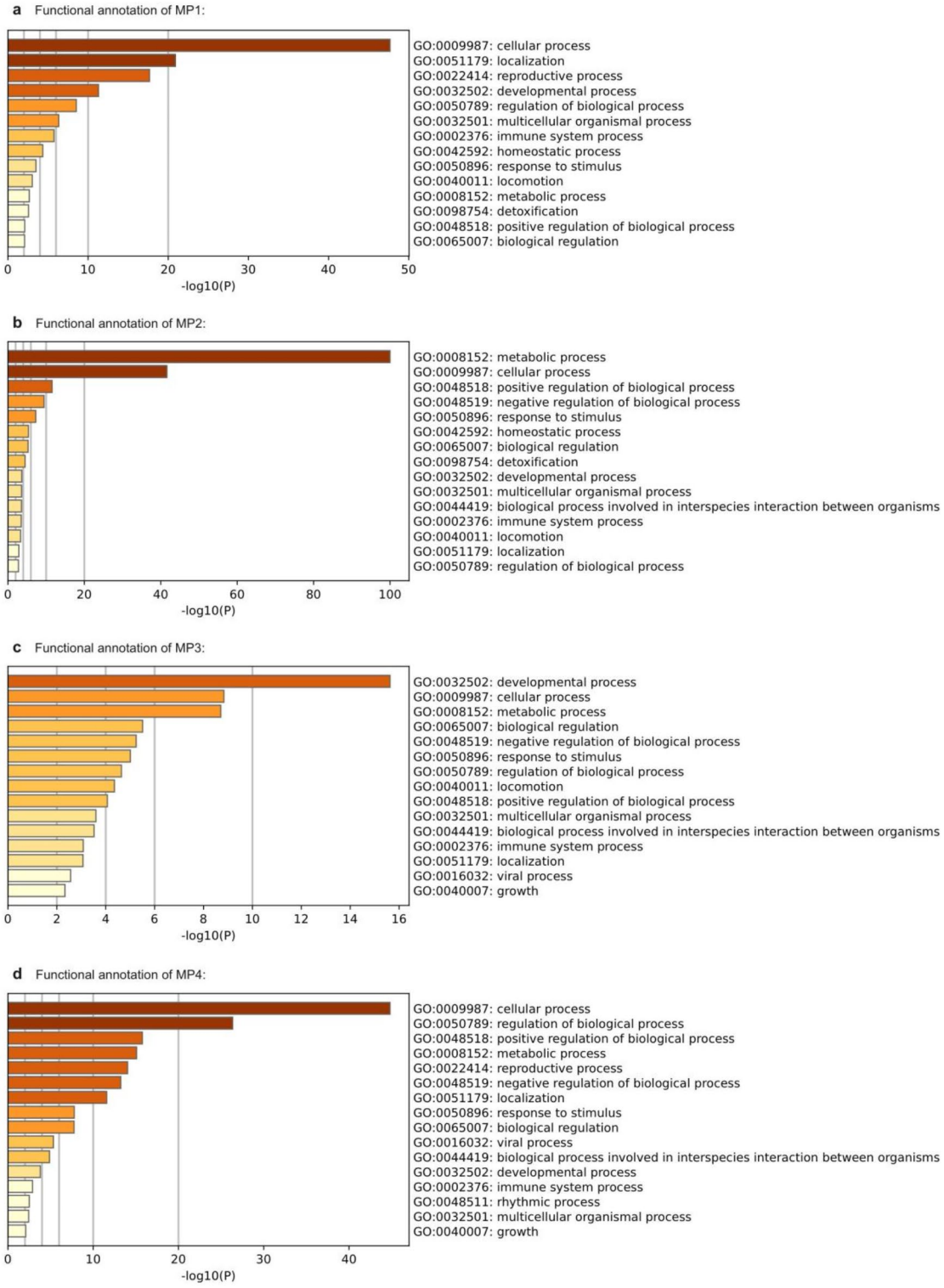

Fig. 6. Gene function analysis of four robust MPs in LUSC. (**a**-**d**) Bar plots depicting the top 15 enriched Gene Ontology (GO) terms associated with the representative genes from MP1 (**a**), MP2 (**b**), MP3 (**c**), and MP4 (**d**) in LUSC.

putative stem cell-like properties, may contribute to tumor initiation and maintenance[67], while deuterosomal cells, involved in tissue repair and regeneration, may play a role in the adaptive responses of the epithelium to the tumorigenic process[68]. Understanding the functional roles of these epithelial subpopulations in LUSC progression could provide novel insights into cancer biology and potential therapeutic targets[69].

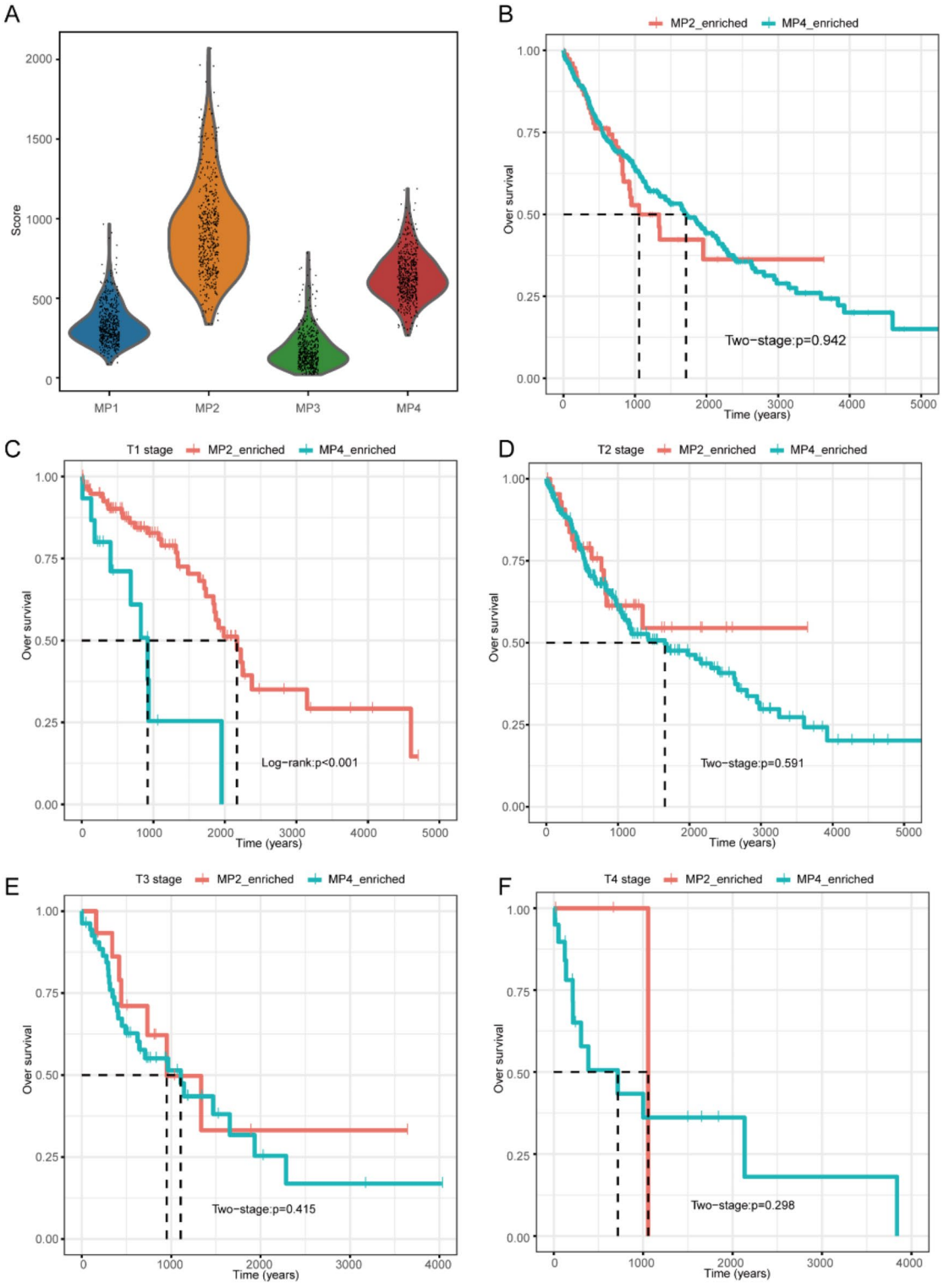

Fig. 7. Clinical implications of MPs in LUSC patients from the TCGA cohort. (**a**) Violin plot displaying the distribution of enrichment scores for all TCGA samples across four MPs. (**b**-**f**) The survival curves illustrate the differences in survival between the MP2 and MP4 clusters across all tumors (**b**), as well as specifically for T1 tumors (**c**), T2 tumors (**d**), T3 tumors (**e**), and T4 tumors (**f**).

To characterize intratumor heterogeneity among malignant cells, we applied NMF programs to scRNA-seq data. We identified four distinct malignant cell phenotypes (MPs) that could be targeted for effective treatments in the majority of LUSC patients. Survival analysis using bulk RNA-seq samples labeled with the highest-scoring MP further highlighted the clinical significance of these MPs. Targeting representative genes of each MP may lead to effective treatments, especially for early-stage LUSC patients.

While the study has shed light on potential therapeutic targets that hold promise for improving patient outcomes, it is imperative to acknowledge the inherent limitations of this research. Firstly, it is important to note that the study focused on a specific subset of LUSC patients, utilizing only three cohorts for analysis. Consequently, the findings may not be entirely representative of the broader LUSC population. To establish the clinical significance of these findings, it is crucial to conduct further investigations involving larger and more diverse patient cohorts. Furthermore, it is worth noting that the study primarily provided correlative observations without extensive functional validation. Although the study identified distinct cell types and subpopulations within the TME, the underlying mechanisms driving these observed cellular changes remain incompletely understood. To address this gap in knowledge, additional experimental studies employing functional assays and animal models are warranted. Such studies would provide valuable insights into the functional relevance of the identified cell types and subpopulations in the progression of LUSC.

In conclusion, this study utilizing scRNA-seq technology has provided valuable insights into the TME of LUSC. By characterizing the cellular composition of the TME and identifying trends in cell type proportions across different tumor stages, this research has shed light on the involvement of specific cell types in LUSC development. The identification of distinct malignant cell phenotypes using NMF programs further highlights the clinical implications of these findings. It is essential for future research endeavors to address the limitations of this study and expand our understanding of this complex ecosystem. By incorporating new techniques and focusing on the specific functions and interactions of different cell types, researchers can pave the way for personalized and more effective treatments for LUSC patients.

Materials and methods

Data acquisition

We downloaded 10X scRNA-seq data of 22 primary LUSC samples from the GSE148071 in Gene Expression Omnibus (GEO) (https://www.ncbi.nlm.nih.gov/)[70], and 50 primary LUSC samples from the dataset of WCH (West China Hospital) (http://lungcancer.chenlulab.com)[71]. The merged scRNA-seq dataset includes 179,506 cells in total. Bulk RNA sequencing (RNA-seq) data and clinicopathological features of LUSC were downloaded from the TCGA-LUSC database[72], and served as an independent validation set for our study. All patient staging classification information from all cohorts is derived from the AJCC TNM classification system developed by the American Joint Committee on Cancer, including 'I,' 'II,' 'III,' and 'unknown.

Preprocessing, clustering and cell type annotation of scRNA-seq data

A Python-based toolkit, Scanpy (version 1.8.2)[73], was used for the downstream analysis of scRNA-seq data. The normalized expression matrix was calculated based on the raw UMI counts after normalizing total counts per cell (library size) and then scaled by 1e6 and logarithmically transformed. Then two datasets were then merged into one, top 2,000 highly variable genes were selected for the following analysis. Dimension reduction and unsupervised clustering were performed according to the standard workflow implemented in Scanpy. Principal component analysis (PCA) was performed on the top 2,000 highly variable genes to reduce noise. To effectively eliminate batch effects between different datasets, we employed the Harmony method to correct the top 20 principal components. This method optimizes the similarity between cells, ensuring that cells from different samples exhibit greater consistency in expression patterns, thereby enhancing data integration and the reliability of subsequent analyses. After addressing the batch effects, we constructed a neighborhood graph using the BBKNN (Batch Balanced KNN) method. This approach accounts for batch effects while learning the joint representation of cells, thereby improving the accuracy of clustering and annotation. The application of BBKNN ensures that cells from different batches are reasonably clustered together in the analysis of cellular similarity. The top 20 principal components were used for graph construction. A k nearest neighbor (KNN) graph was then constructed based on the Euclidean distance in PCA space, and the edge weights between any two cells were refined based on the shared overlap in their local neighborhoods. Leiden algorithm[23] was applied to the KNN graph to detect communities. The top 20 principal components were also used for non-linear dimension reduction to generate the Uniform Manifold Approximation and Projection (UMAP) for visualization. We annotated each cell cluster according to well-known cell markers provided by original literatures [71 72], resulting in a total of seven major cell types, including T cell, B cell, epithelial cell, endothelial cell, mast cell, myeloid cell, and fibroblast.

Identifying malignant cells

Identification Method for Malignant Cells: We identified malignant cells by assessing the copy number variation (CNV) characteristics within the dataset. Our hypothesis is that epithelial cells with elevated CNV levels are more likely to be malignant.

Tools Used: We utilized a sliding window approach with the infercnvpy package[24], which is specifically designed to determine CNV characteristics for all cells.

Normal Reference Cell Types: Our normal reference cells included T cells, B cells, myeloid cells, and mast cells. By comparing these normal reference cells, we observed that a subset of epithelial cells exhibited significantly higher CNV burdens than the normal cells.

Cell Clustering Analysis: Clustering analysis of CNV characteristics across 179,506 cells enabled us to identify 9,611 malignant cells, effectively distinguishing them from non-malignant epithelial cells.

Identification of subpopulations in the major cell type

Next, we performed a second round of unsupervised clustering on some major cell types to obtain the subpopulations within T cells, epithelial cells and myeloid cells in LUSC. The second-round clustering procedure was the same as the first-round clustering. It started with a normalized expression matrix, calculated PCA, constructed the KNN graph, detected cell clusters by Leiden algorithm, performed dimensionality reduction for visualization, and identified subpopulations based on the marker genes.

Cell proportion analysis

To investigate whether the proportion of a specific cell type or subpopulation within the TME differs significantly between the patient groups of different tumor stages, we performed a one-way analysis of variance (ANOVA) on scRNA-seq data. In addition, we applied the Propeller method, a robust and flexible approach that leverages biological replicates to test for differences in cell type proportions in single-cell data. This method involves applying a logit transformation to the proportions, followed by ANOVA for differential testing[74]. To explore the prediction values of cell type proportions in the tumor stage, we applied T-test to the bulk RNA-seq data. Both tests were conducted using the SciPy v1.10.1 Python package[75].

Defining NMF programs

We carried out non-negative matrix factorization (NMF), which is an algorithm for multivariate analysis and linear algebra, for malignant cells from each tumor sample separately to generate gene and cell programs that capture the heterogeneity of malignant cells within each tumor sample[76]. For any given non-negative matrix V, the NMF algorithm can find a non-negative matrix W and a non-negative matrix H, so that a non-negative matrix can be decomposed into the product of two non-negative matrices. As the NMF algorithm requires a parameter K to control the number of resulting programs, we ran NMF with different K values (K = 5, 6, 7, 8, 9, and 10). Then we determined the best K value which has the biggest ratio of stability to prediction-error and obtained the most stable NMF programs for each sample. This approach yielded a total of 468 NMF programs, and each NMF program was summarized by the top 50 genes based on NMF coefficients.

Defining MPs

We proceeded to cluster these 468 NMF programs based on their top 50 genes to derive the meta-programs (MPs). In essence, each NMF program was compared to all other NMF programs to evaluate the extent of gene overlap between them. If two NMF programs shared 10 or more genes, it was inferred that they might belong to a common MP. A reproducible MP was defined when the number of overlapping NMF programs (with > 10 shared genes) exceeded 5 instances, indicating that this MP was present in over 10% of the tumor samples and thus deemed reproducible. The genes encompassed within the reproducible MP were a combination of genes associated with all NMF programs linked to that particular MP. Through this approach, we identified four distinct reproducible MPs, and subsequently assessed their enrichment in functionally annotated gene sets.

Survival analysis

The bulk RNA-seq data from the TCGA-LUSC cohort was initially normalized using the Transcripts Per Million (TPM) method prior to analysis. To assess the enriched MPs in each sample from the TCGA-LUSC cohort, the genes belonging to the four MPs were utilized. The enrichment score of every MP for a sample was achieved by employing Scanpy's score_genes function. Subsequently, each sample was assigned to the MP group with the highest enrichment score. For samples in each MP group, the R packages "survminer" (v.0.4.9) and "survival" (v.3.4.0) were employed to generate Kaplan-Meier (KM) curves. These curves were used to visualize the survival data and determine the impact of each cell type on overall survival. For significance testing, the default log-rank test is applied when the survival curves do not cross; otherwise, we implement a two-stage procedure.

Data availability

The raw and processed single-cell RNA sequencing data utilized in this study have been deposited into the Gene Expression Omnibus (GEO) database under accession number GSE148071 and the West China Hospital (WCH) institutional database with appropriate access permissions. All relevant datasets, including normalized gene expression matrices, cell cluster annotations, and metadata, are publicly accessible for research purposes. Source code for computational analyses and custom scripts used in the study are available on GitHub (https://github.com/author_username/LUSC_scRNAseq_analysis).Detailed information on how to access and reproduce the computational workflow is provided in the repository's documentation. For inquiries regarding additional data or resources not covered in the public repositories, please contact the corresponding author.

Received: 16 May 2024; Accepted: 10 March 2025
Published online: 26 March 2025

References

1. Bray, F. et al. Global cancer statistics 2018: GLOBOCAN estimates of incidence and mortality worldwide for 36 cancers in 185 countries. *CA Cancer J. Clin.* **68** (6), 394–424 (2018).
2. Herbst, R. S., Morgensztern, D. & Boshoff, C. The biology and management of non-small cell lung cancer. *Nature* **553** (7689), 446–454 (2018).
3. Ohue, Y. & Nishikawa, H. Regulatory T (Treg) cells in cancer: can Treg cells be a new therapeutic target? *Cancer Sci.* **110** (7), 2080–2089 (2019).
4. Chen, S. et al. Introduction of exogenous wild–type p53 mediates the regulation of oncoprotein 18/stathmin signaling via nuclear factor–κB in non–small cell lung cancer NCI–H1299 cells. *Oncol. Rep.* **41** (3), 2051–2059 (2019).

5. Yang, M. et al. A multi-omics machine learning framework in predicting the survival of colorectal cancer patients. *Comput. Biol. Med.* **146**, 105516 (2022).
6. Ma, X. et al. A machine Learning-based diagnosis of thyroid cancer using thyroid nodules ultrasound images. *Curr. Bioinform.* **15** (4), 349–358 (2020).
7. Peng, P. et al. Prognostic factors in stage IV colorectal cancer patients with resection of liver and/or pulmonary metastases: A Population-Based cohort study. *Front. Oncol.* **12**, 850937 (2022).
8. Meng, H. et al. Genomic profiling of driver gene mutations in Chinese patients with Non-Small cell lung cancer. *Front. Genet.* **10**, 1008 (2019).
9. Binnewies, M. et al. Understanding the tumor immune microenvironment (TIME) for effective therapy. *Nat. Med.* **24** (5), 541–550 (2018).
10. Ostman, A. The tumor microenvironment controls drug sensitivity. *Nat. Med.* **18** (9), 1332–1334 (2012).
11. Gandhi, L. et al. Pembrolizumab plus chemotherapy in metastatic Non-Small-Cell lung cancer. *N Engl. J. Med.* **378** (22), 2078–2092 (2018).
12. Nadal, E. et al. Immunotherapy with checkpoint inhibitors in non-small cell lung cancer: insights from long-term survivors. *Cancer Immunol. Immunother.* **68** (3), 341–352 (2019).
13. Baslan, T. & Hicks, J. Unravelling biology and shifting paradigms in cancer with single-cell sequencing. *Nat. Rev. Cancer.* **17** (9), 557–569 (2017).
14. Zhuang, J. et al. A novel Single-Cell RNA sequencing data feature extraction method based on gene function analysis and its applications in glioma study. *Front. Oncol.* **11**, 797057 (2021).
15. Lambrechts, D. et al. Phenotype molding of stromal cells in the lung tumor microenvironment. *Nat. Med.* **24** (8), 1277–1289 (2018).
16. Yang, J., Liao, B., Zhang, T., Xu, Y. & Editorial Bioinformatics analysis of single cell sequencing data and applications in precision medicine. *Front. Genet.* **10**, 1358 (2019).
17. Guo, X. et al. Global characterization of T cells in non-small-cell lung cancer by single-cell sequencing. *Nat. Med.* **24** (7), 978–985 (2018).
18. Zilionis, R. et al. Single-Cell transcriptomics of human and mouse lung cancers reveals conserved myeloid populations across individuals and species. *Immunity* **50** (5), 1317–1334e1310 (2019).
19. Goveia, J. et al. An integrated gene expression landscape profiling approach to identify lung tumor endothelial cell heterogeneity and angiogenic candidates. *Cancer Cell.* **37** (1), 21–36e13 (2020).
20. Salcher, S. et al. High-resolution single-cell atlas reveals diversity and plasticity of tissue-resident neutrophils in non-small cell lung cancer. *Cancer Cell.* **40** (12), 1503–1520e1508 (2022).
21. Korsunsky, I. et al. Fast, sensitive and accurate integration of single-cell data with harmony. *Nat. Methods.* **16** (12), 1289–1296 (2019).
22. Polanski, K. et al. BBKNN: fast batch alignment of single cell transcriptomes. *Bioinformatics* **36** (3), 964–965 (2020).
23. Traag, V. A., Waltman, L. & van Eck, N. J. From Louvain to Leiden: guaranteeing well-connected communities. *Sci. Rep.* **9** (1), 5233 (2019).
24. Patel, A. P. et al. Single-cell RNA-seq highlights intratumoral heterogeneity in primary glioblastoma. *Science* **344** (6190), 1396–1401 (2014).
25. Komi, D. E. A. & Redegeld, F. A. Role of mast cells in shaping the tumor microenvironment. *Clin. Rev. Allergy Immunol.* **58** (3), 313–325 (2019).
26. Aponte-López, A. Muñoz-Cruz,Samira. Mast cells in the tumor microenvironment. *Adv. Exp. Med. Biol.* **1273**, 159–173 (2020).
27. Lv, Y. et al. Increased intratumoral mast cells foster immune suppression and gastric cancer progression through TNF-α-PD-L1 pathway. *J. Immunother. Cancer* **7**(1), 54 (2019).
28. Espinosa-Riquer, Z. P. et al. Signal transduction pathways activated by innate immunity in mast cells: translating sensing of changes into specific responses. *Cells* **9**(11), 2411 (2020).
29. DeLeon-Pennell, K. Y., Barker, T. H. & Lindsey, M. L. Fibroblasts: the arbiters of extracellular matrix remodeling. *Matrix Biol.* **91–92**, 1–7 (2020).
30. Mao, X. et al. Crosstalk between cancer-associated fibroblasts and immune cells in the tumor microenvironment: new findings and future perspectives. *Mol. Cancer* **20**(1), 131 (2021).
31. Shiga, K. et al. Cancer-Associated fibroblasts: their characteristics and their roles in tumor growth. *Cancers* **7** (4), 2443–2458 (2015).
32. Richard, A. C., Ma, C. Y., Marioni, J. C. & Griffiths, G. M. Cytotoxic T lymphocytes require transcription for infiltration but not target cell Lysis. *EMBO Rep.* **24** (11), e57653 (2023).
33. Zuo, Z., Yin, H., Zhang, Y., Xie, C. & Wang, Q. A cytotoxic T cell inspired oncolytic nanosystem promotes lytic cell death by lipid peroxidation and elicits antitumor immune responses. *Nat. Commun.* **14** (1), 5456 (2023).
34. Shan, F., Somasundaram, A., Bruno, T. C., Workman, C. J. & Vignali, D. A. A. Therapeutic targeting of regulatory T cells in cancer. *Trends Cancer.* **8** (11), 944–961 (2022).
35. Mao, X. et al. Tissue resident memory T cells are enriched and dysfunctional in effusion of patients with malignant tumor. *J. Cancer.* **14** (7), 1223–1231 (2023).
36. Speiser, D. E., Chijioke, O., Schaeuble, K. & Munz, C. CD4(+) T cells in cancer. *Nat. Cancer.* **4** (3), 317–329 (2023).
37. Cenerenti, M., Saillard, M., Romero, P. & Jandus, C. The era of cytotoxic CD4 T cells. *Front. Immunol.* **13**, 867189 (2022).
38. Meiser, P. et al. A distinct stimulatory cDC1 subpopulation amplifies CD8(+) T cell responses in tumors for protective anti-cancer immunity. *Cancer Cell.* **41** (8), 1498–1515e1410 (2023).
39. Mitchell, D., Chintala, S. & Dey, M. Plasmacytoid dendritic cell in immunity and cancer. *J. Neuroimmunol.* **322**, 63–73 (2018).
40. Coillard, A. & Segura, E. In vivo differentiation of human monocytes. *Front. Immunol.* **10**, 1907 (2019).
41. Olingy, C. E., Dinh, H. Q. & Hedrick, C. C. Monocyte heterogeneity and functions in cancer. *J. Leukoc. Biol.* **106**(2), 309–322 (2019).
42. Anderson, N. R., Minutolo, N. G., Gill, S. & Klichinsky, M. Macrophage-Based approaches for cancer immunotherapy. *Cancer Res.* **81** (5), 1201–1208 (2021).
43. Xu, F. et al. Astragaloside IV inhibits lung cancer progression and metastasis by modulating macrophage polarization through AMPK signaling. *J. Exp. Clin. Cancer Res.* **37** (1), 207 (2018).
44. Maynard, A. et al. Therapy-Induced evolution of human lung cancer revealed by Single-Cell RNA sequencing. *Cell* **182** (5), 1232–1251 (2020). e1222.
45. Sarode, P. et al. Epithelial cell plasticity defines heterogeneity in lung cancer. *Cell. Signal.* **65**, 109463 (2020).
46. Guillot, L. et al. Alveolar epithelial cells: master regulators of lung homeostasis. *Int. J. Biochem. Cell. Biol.* **45** (11), 2568–2573 (2013).
47. Barbry, P., Cavard, A., Chanson, M., Jaffe, A. B. & Plasschaert, L. W. Regeneration of airway epithelial cells to study rare cell States in cystic fibrosis. *J. Cyst. Fibros.* **19** (Suppl 1), S42–S46 (2020).
48. Mollaoglu, G. et al. The Lineage-Defining transcription factors SOX2 and NKX2-1 determine lung cancer cell fate and shape the tumor immune microenvironment. *Immunity* **49** (4), 764–779e769 (2018).
49. Zhou, Y. et al. Single-cell RNA landscape of intratumoral heterogeneity and immunosuppressive microenvironment in advanced osteosarcoma. *Nat. Commun.* **11** (1), 6322 (2020).

50. Hall, A. The cytoskeleton and cancer. *Cancer Metastasis Rev.* **28** (1–2), 5–14 (2009).
51. Pelletier, J., Thomas, G. & Volarevic, S. Ribosome biogenesis in cancer: new players and therapeutic avenues. *Nat. Rev. Cancer*. **18** (1), 51–63 (2018).
52. Li, J., Tang, L. L. & Ma, J. Survival-related indicators ALOX12B and SPRR1A are associated with DNA damage repair and tumor microenvironment status in HPV 16-negative head and neck squamous cell carcinoma patients. *BMC Cancer*. **22** (1), 714 (2022).
53. Icard, P., Fournel, L., Wu, Z., Alifano, M. & Lincet, H. Interconnection between metabolism and cell cycle in cancer. *Trends Biochem. Sci.* **44** (6), 490–501 (2019).
54. Jamasbi, E., Hamelian, M., Hossain, M. A. & Varmira, K. The cell cycle, cancer development and therapy. *Mol. Biol. Rep.* **49** (11), 10875–10883 (2022).
55. Ostroumov, D., Fekete-Drimusz, N., Saborowski, M., Kühnel, F. & Woller, N. CD4 and CD8 T lymphocyte interplay in controlling tumor growth. *Cell. Mol. Life Sci.* **75** (4), 689–713 (2017).
56. Chow, A., Perica, K., Klebanoff, C. A. & Wolchok, J. D. Clinical implications of T cell exhaustion for cancer immunotherapy. *Nat. Reviews Clin. Oncol.* **19** (12), 775–790 (2022).
57. Togashi, Y., Shitara, K. & Nishikawa, H. Regulatory T cells in cancer immunosuppression — implications for anticancer therapy. *Nat. Reviews Clin. Oncol.* **16** (6), 356–371 (2019).
58. Tanaka, A. & Sakaguchi, S. Regulatory T cells in cancer immunotherapy. *Cell Res.* **27** (1), 109–118 (2016).
59. Cui, C., Lan, P. & Fu, L. The role of myeloid-derived suppressor cells in Gastrointestinal cancer. *Cancer Commun.* **41**(6), 442–471 (2021).
60. Shrihari, T. G. Dual role of inflammatory mediators in cancer. *Ecancermedicalscience* **11**, 721 (2017).
61. Caronni, N., Savino, B. & Bonecchi, R. Myeloid cells in cancer-related inflammation. *Immunobiology* **220** (2), 249–253 (2015).
62. Hilligan, K. L. & Ronchese, F. Antigen presentation by dendritic cells and their instruction of CD4 + T helper cell responses. *Cell Mol. Immunol.* **17** (6), 587–599 (2020).
63. Rotman, J. et al. Adenocarcinoma of the uterine cervix shows impaired recruitment of cDC1 and CD8 + T cells and elevated β-Catenin activation compared with squamous cell carcinoma. *Clin. Cancer Res.* **26** (14), 3791–3802 (2020).
64. Oshi, M. et al. Plasmacytoid dendritic cell (pDC) infiltration correlate with tumor infiltrating lymphocytes, cancer immunity, and better survival in triple negative breast cancer (TNBC) more strongly than conventional dendritic cell (cDC). *Cancers* **12**(11), 3342 (2020).
65. Pénzes, Z. et al. The dual role of Cannabidiol on monocyte-derived dendritic cell differentiation and maturation. *Front. Immunol.* **14**, 1240800 (2023).
66. Lee, H-W., Choi, H-J., Ha, S-J., Lee, K-T. & Kwon, Y-G. Recruitment of monocytes/macrophages in different tumor microenvironments. *Biochim. Et Biophys. Acta (BBA) - Reviews Cancer*. **1835**(2), 170–179 (2013).
67. Hynds, R. E. & Janes, S. M. Airway basal cell heterogeneity and lung squamous cell carcinoma. *Cancer Prev. Res.* **10** (9), 491–493 (2017).
68. Davis, J. D. & Wypych, T. P. Cellular and functional heterogeneity of the airway epithelium. *Mucosal Immunol.* **14** (5), 978–990 (2021).
69. Rooney, C. & Sethi, T. The epithelial cell and lung cancer: the link between chronic obstructive pulmonary disease and lung cancer. *Respiration* **81** (2), 89–104 (2011).
70. Wu, F. et al. Single-cell profiling of tumor heterogeneity and the microenvironment in advanced non-small cell lung cancer. *Nat. Commun.* **12** (1), 2540 (2021).
71. Zhang, L. et al. Integrated single-cell RNA sequencing analysis reveals distinct cellular and transcriptional modules associated with survival in lung cancer. *Signal. Transduct. Target. Ther.* **7** (1), 9 (2022).
72. Cancer Genome Atlas Research N et al. The cancer genome atlas Pan-Cancer analysis project. *Nat. Genet.* **45** (10), 1113–1120 (2013).
73. Wolf, F. A., Angerer, P. & Theis, F. J. SCANPY: large-scale single-cell gene expression data analysis. *Genome Biol.* **19** (1), 15 (2018).
74. Phipson, B. et al. Propeller: testing for differences in cell type proportions in single cell data. *Bioinformatics* **38** (20), 4720–4726 (2022).
75. Virtanen, P. et al. SciPy 1.0: fundamental algorithms for scientific computing in python. *Nat. Methods*. **17** (3), 261–272 (2020).
76. Gavish, A. et al. Hallmarks of transcriptional intratumour heterogeneity across a thousand tumours. *Nature* **618** (7965), 598–606 (2023).

Author contributions

C.H designed the study; J.F, Y.C, Y. G and R.H performed the study, and analyzed the data; H.S and Y.Z performed literature search and interpreted the data. R.H and Y.G wrote the manuscript; X.D contributed to the manuscript editing; all other authors reviewed and approved the final version of the manuscript.

Declarations

Competing interests

The authors declare no competing interests.

Additional information

Supplementary Information The online version contains supplementary material available at https://doi.org/10.1038/s41598-025-93916-3.

Correspondence and requests for materials should be addressed to C.H.

Reprints and permissions information is available at www.nature.com/reprints.

Publisher's note Springer Nature remains neutral with regard to jurisdictional claims in published maps and institutional affiliations.

Open Access This article is licensed under a Creative Commons Attribution-NonCommercial-NoDerivatives 4.0 International License, which permits any non-commercial use, sharing, distribution and reproduction in any medium or format, as long as you give appropriate credit to the original author(s) and the source, provide a link to the Creative Commons licence, and indicate if you modified the licensed material. You do not have permission under this licence to share adapted material derived from this article or parts of it. The images or other third party material in this article are included in the article's Creative Commons licence, unless indicated otherwise in a credit line to the material. If material is not included in the article's Creative Commons licence and your intended use is not permitted by statutory regulation or exceeds the permitted use, you will need to obtain permission directly from the copyright holder. To view a copy of this licence, visit http://creativecommons.org/licenses/by-nc-nd/4.0/.

© The Author(s) 2025